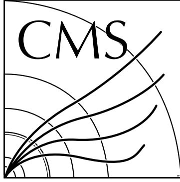

The Compact Muon Solenoid Experiment

CMS Note

Mailing address: CMS CERN, CH-1211 GENEVA 23, Switzerland

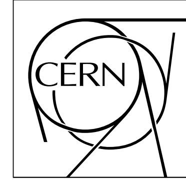

CMS NOTE 2000-061
Octobers 18, 2000

Silicon sensors for the CMS Preshower

Anna Peisert[1] and Nikolai Zamiatin[2]

[1]CERN, [2]JINR

for the Preshower Group

Abstract

The paper is a summary of a research and development program, conducted during the past three years on the CMS Preshower silicon sensors with the goal at defining the specifications. The main point was the radiation hardness of these devices, resulting from the specific design, metal lines wider than the p^+ implants and a series of guard rings, and to the production technology, a deep n^+ layer on the ohmic side. An acceptable noise and a uniform charge collection were guaranteed by an appropriate choice of the interstrip region width. About 65 sensors, of different designs and coming from six manufacturers, were irradiated with neutrons and protons and thoroughly tested before and after irradiation. The results of the tests and the final specifications are presented.

1 INTRODUCTION

The main purpose of the Endcap Preshower detector of the CMS experiment [1] is to separate photons from neutral pions (2 close photons) in the rapidity range 1.65 to 2.6. Thin lead radiators initiate the electromagnetic showering process. The photon / neutral pion separation is obtained by an analysis of the spatial distribution of the energy deposited in position sensitive detectors following the lead radiators.

We have chosen silicon sensors as active elements because of their very fast and linear response, even in the dense core of the shower. The average profile of an electron shower after two radiation lengths is shown on figure 1. It shows both a very narrow (~100 µm) core and long tails. Simulation studies have shown that a ~2 mm granularity of the sensitive detectors is optimal to perform the γ/π^0 separation. Each endcap of the Preshower detector contains two orthogonal planes of silicon strip detectors with 1.9 mm pitch.

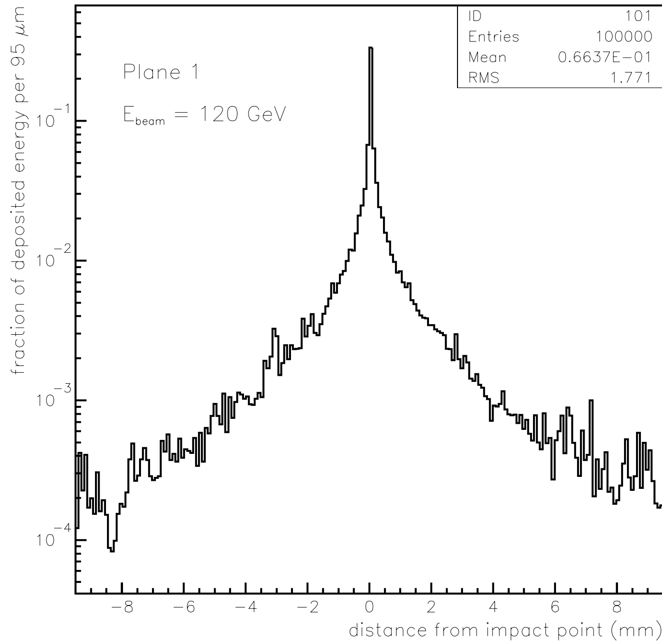

Figure 1: Transverse profile of an electron shower after two radiation lengths.

Not only the spatial shape, but also a precise, typically 5% accuracy, measurement of the energy deposited in the silicon is required for a good Preshower performance. This energy measurement is used to estimate the energy lost in the lead and to recover the good energy resolution of the crystal electromagnetic calorimeter, which follows the Preshower. The silicon sensors must therefore have a good, spatially uniform charge collection efficiency. Moreover, the charge calibration of the sensors will be performed with single minimum ionizing particles and for this measurement a low noise is absolutely crucial.

The integrated fluence of charged hadrons and neutrons above 100 keV in the centre of the Preshower detector will reach ~2 x 10^{14} particles/cm^2 after 10 years of operation with 85% of them being neutrons. The silicon sensors will suffer from radiation damage, in which the n bulk will undergo type inversion and then become less and less resistive, requiring a higher and higher operational voltage. The leakage current, the breakdown voltage and the charge collection efficiency of heavily irradiated detectors are therefore important and they have to be considered in the design.

In section 2 we describe the Preshower sensor design. The measurement set-ups and the irradiation facilities are presented in section 3. Results of measurements of irradiated and non irradiated detectors are shown in section 4. Section 5 describes the technological issues related to the production of silicon sensors and the specifications are summarized in section 6. The last section is reserved for a summary and conclusions.

2 GENERAL SENSOR DESIGN

The overall cost of the Preshower was kept in mind during the design process of the sensors and electronics. The total sensitive area of 17 m^2 is built out of 4304 identical, square sensors, so there is only one set of masks to be designed and produced. The sensors are made on 4" wafers, the technology available in all foundries of the collaborating countries. They have a total area of 63x63 mm^2 with 32 strips at 1.9 mm pitch. Again for cost effectiveness the p^+ strips are directly coupled to the aluminum readout lines and the front-end electronics includes a leakage current compensation mechanism to keep the baseline level low. In total there are only four masks, including the passivation.

The effects of radiation that have to be taken into account are the increase of the leakage current and the silicon type inversion and a progressive increase of the full depletion voltage. The leakage current increases linearly with fluence with a constant $\alpha = 3 \times 10^{-17}$ A/cm [2], [3]. We calculate the total current per detector in the center of the Preshower to be around 600 μA after 2×10^{14} n/cm^2 at -5 ^{o}C. It corresponds to about 20 μA per strip and it has to be taken into account in the readout chip design.

The effective doping concentration changes due to two effects: removal of the donor atoms and the creation of acceptors. At a fluence of the order of $.3 \times 10^{14}$ n/cm^2 their numbers are equal and silicon becomes intrinsic. From that point on the number of acceptors is higher than the number of donors and silicon becomes p-type. The effective doping concentration increases linearly with fluence and so does the full depletion voltage [4]. We expect the operating voltage to be of the order of 400 V for the highest fluence, so the detectors should hold at least 500 V to have a reasonably long efficiency plateau.

The high voltage performance was a key issue in the detector design. In order to guarantee a high breakdown voltage, we designed the metal lines .01 mm wider than the p^+ lines. This design is known to give a lower maximum field around the edges of the p^+ lines [5], [6]. A series of four guard rings was implemented to protect the active area from the currents generated at the edges of the sensor.

Figures 2 and 3 show the layout and the cross section of the Preshower sensors.

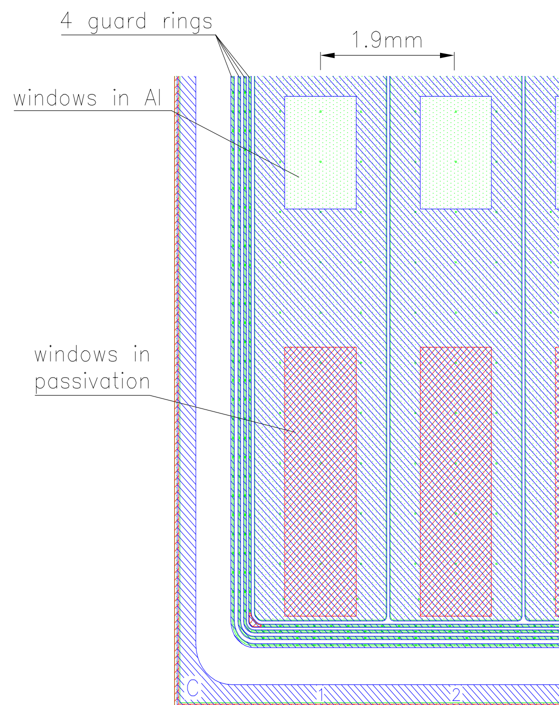

Figure 2: Layout of a Preshower Si sensor.

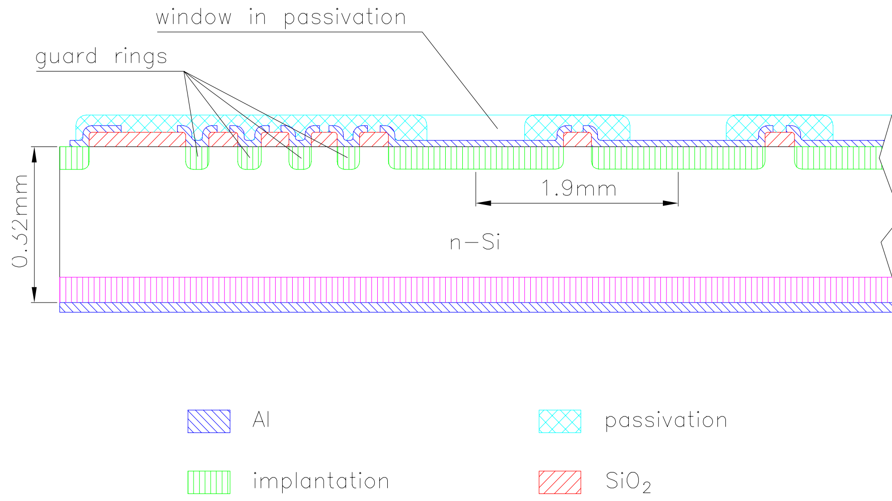

Figure 3: Cross section of a Preshower Si sensor.

While the total sensor area and the strip pitch was fixed by the choice of the wafer size, the strip width was optimized from the noise and charge collection uniformity points of view. During a physics run, e.g. the shower measurements, the charge collection uniformity is crucial, while the noise is relatively less important, because the charge deposited by electrons of energies higher than 20 GeV corresponds to several tens of minimum ionizing particles. For the calibration, on the other hand, it is essential to have a low noise and to be able to detect single particles. These two requirements are in competition, because, as we will show later, the best charge collection uniformity can be obtained with narrow interstrip gaps, which in turn result in a higher capacitance and a higher noise. Calculations using two independent methods [6], [7] have shown that one can reduce the interstrip capacitance by about 5 pF by increasing the strip distance from .04 mm to .16 mm.

The Preshower custom designed readout chip, PACE [8], contains 32 channels of preamplifiers, each followed by a shaper with selectable gain: a low gain for shower measurements and a high gain for calibration with minimum ionizing particles, with a possibility to switch remotely from one to the other. The peaking time is 25 ns, dictated by the frequency of the LHC beam interactions. The amplified and shaped signal is stored in an analog data buffer, 160 cells deep, waiting for the decision from the level 1 trigger. Voltage from selected events is then read out through a multiplexer.

The preamplifier noise is expected to be [9]:

$$ENC_{preamplifier} = 640\ e^{-} + 33\ e^{-}/pF \times \mathrm{C}$$

where C is the total strip capacitance. The strip capacitance is the sum of the capacitance to the backplane and of the direct capacitance to the adjacent strips. For a Preshower sensor it is dominated by the backplane, because of its large surface area. For a 1.9 x 61 mm^2 strip we expect 40 pF to 45 pF depending on the thickness. To that one should add 5 pF to 10 pF of interstrip capacitance, depending on the design. The amplifier noise, including the load capacitance, is therefore expected to be around 2300 e^-.

The analog memory DC level is not perfectly uniform and its contribution is of the order of 1 mV, independent of the detector parameters. At high shaper gain, 32mV/4fC, it corresponds to about 780 e^- and is negligible compared to the preamplifier noise. At low shaper gain, 4mV/4fC, it is about 6250 e^- and becomes dominant. But the low gain state will be used for shower measurements, where the signal will be several minimum ionizing particles. So in this case the signal to noise ratio will be sufficiently high.

The detector contributes to the noise through the leakage current and the parallel and series resistances. The contribution from the leakage current will be relatively small at the beginning, as the PACE peaking time is very short. For an average current of 100 nA per strip, we calculate 170 electrons of noise. This contribution will increase progressively to reach 2400 electrons at the end of the LHC operation. We do not expect an increase of the capacitance with time and radiation damage, but there will be a charge loss corresponding to about 15% [10], [11], [12] after an equivalent fluence of 2 x 10^{14} n/cm^2. The overall signal to noise ratio will decrease with time.

The contribution from the parallel resistance is negligible as it is almost infinite for DC coupled sensors. The series resistance, 2 Ω for a 6 cm long Al strip, is very low in our design and its contribution will also be negligible.

3 MEASUREMENT SET-UP AND IRRADIATION FACILITIES

3.1 C-V and I-V measurements

The leakage current is measured using a Keithley 237 High Voltage Source Measure Unit, which can supply up to 1100 V. Typically we measure the current up to 500 V on non-irradiated detectors and up to 1000 V on irradiated ones. Non irradiated detectors are tested at room temperature and the irradiated ones at temperatures below 0^oC.

The same voltage source is used for biasing the detectors for the capacitance measurements, which is done with the HP 4284A Precision LCR Meter. The meter has a generator with a variable frequency in the range between 20 Hz and 1 MHz and a variable amplitude of up to 1 V. It measures two out of three variables: L, C and R and one can assume a series or parallel connection of the two elements. We usually measure C and R connected in parallel.

For the depletion layer capacitance all the strips are bonded together and the capacitance is measured between the strips and the backplane. A special circuit is used to decouple the high voltage from the input of the meter. One can also measure the capacitance for each strip separately. The result is the same, but the measurement takes much longer.

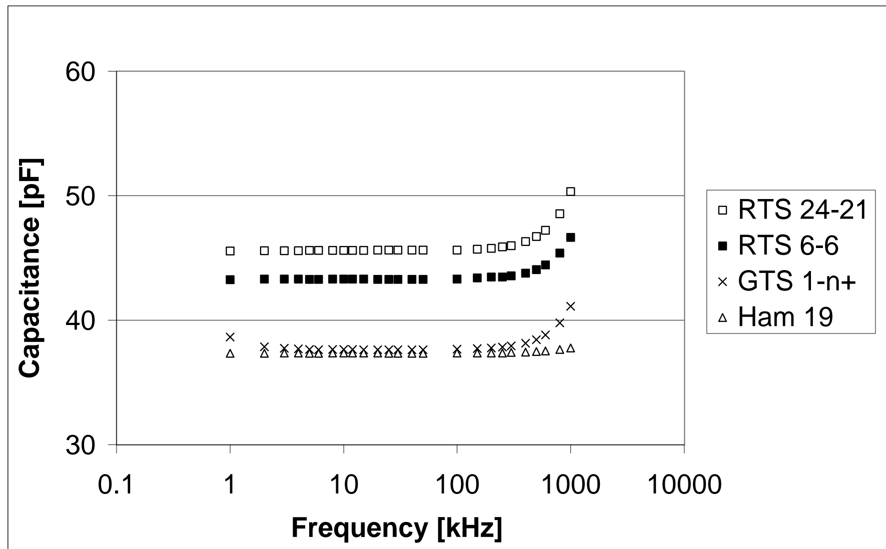

Figure 4: Strip capacitance to the backplane at full depletion voltage as a function of frequency for three detectors of different area and thickness.

Figure 4 shows the backplane capacitance as a function of frequency for three detectors measured at 50 V above the full depletion voltage. The difference of values corresponds to different areas and thicknesses (see table 1) of the sensors. The capacitance is constant in the range of a few kHz up to about 300 kHz and its value corresponds to the geometrical capacitance. It increases at higher frequencies. The frequency dependence of the capacitance of a ceramic capacitor is shown as a reference.

The full depletion voltage is determined from the C-V plot and is defined as the voltage at which the capacitance reaches the minimum. For non-irradiated detectors this voltage does not depend on the frequency, but on irradiated and inverted detectors it is a strong function of frequency, due to a lower charge-carrier mobility. Figure 5 shows the total detector capacitance (32 strips in parallel) as a function of voltage for a non-irradiated detector (left) and a detector irradiated to 1.4 x 10^{14} n/cm^2 (right). The voltage dependence of the capacitance of the non-irradiated detector is the same between 1 kHz and 100 kHz and the full depletion voltage does not depend on frequency. For the irradiated sensor, however, the shape of the C-V curve strongly depends on the frequency and so does the full depletion voltage. We use the 5 kHz generator for the depletion layer capacitance measurements for all detectors in order to be able to compare our results with others [13].

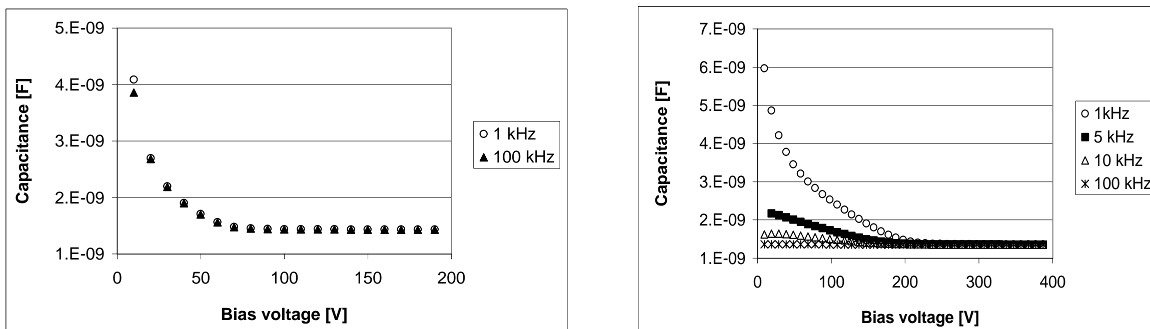

Figure 5: Depletion layer capacitance as a function of voltage for a non-irradiated detector (left) and for a detector irradiated to 1.4 x 10^{14} n/cm^2 (right) for different measurement frequencies.

For the total strip capacitance we bond 31 strips together, leaving one, in the center, free. The capacitance is measured between this strip and the group of 31. Figure 6 shows the schematic set-up.

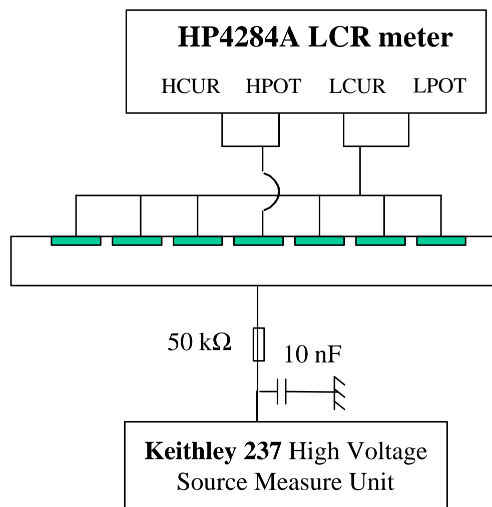

Figure 6: Set-up used to measure the total strip capacitance to its neighbors and to the backplane.

The total strip capacitance is an important parameter, because the noise strongly depends on it. Ideally it should be measured at a frequency at which the readout electronics is sensitive, 40 MHz in our case, but the highest frequency we were able to use is 1 MHz. In order to get an idea whether the capacitance measured at 1 MHz is far from the one at 40 MHz, we plotted the noise, measured at 40 MHz as a function of the capacitance. We used the SCT32 chip[14] with a peaking time of 25 ns, similar to PACE, for this measurement. Figure 7 shows the results of measurements for detectors and for a series of passive capacitors. The agreement is very good and we consider the values measured at 1 MHz as valid for the noise calculations.

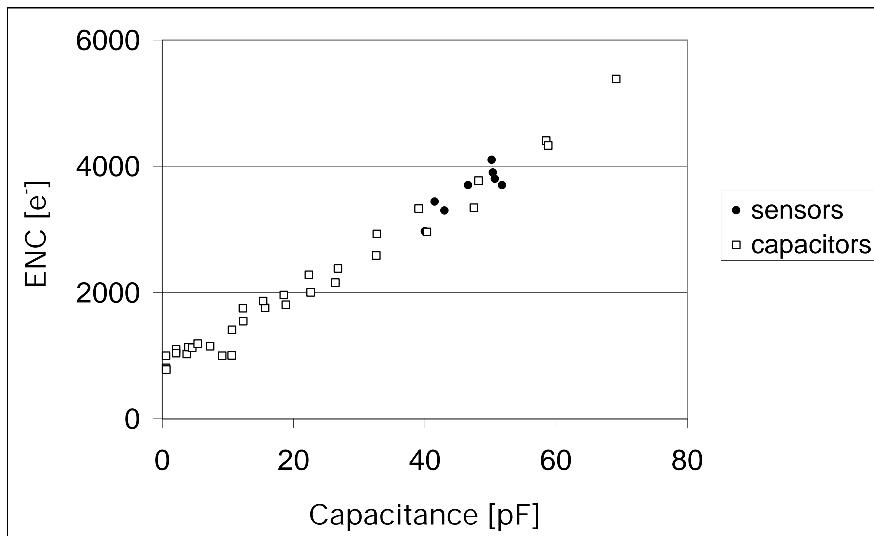

Figure 7: Noise measured with the SCT32 chip as a function of capacitance, measured at 1 MHz, for detectors and for a series of passive capacitors.

3.2 Tests with particles

The response of silicon sensors to particles has been tested using the SCT32 and SCT128[14] chips. They have 32 and 128 channels, respectively, and a peaking time of 25 ns. 3.5 MeV electrons from a collimated ^{106}Ru source traverse the detector and are detected in a scintillator by two photomultipliers [15]. The coincidence of the PM signals is used as a trigger. The collected charge is almost the same as that of a minimum-ionizing particle and follows a Landau distribution. Our signal is defined as the most probable value of this distribution. The charge collected from irradiated detectors is normalized to the signal from a .3 mm thick, non-irradiated sensor at 500 V. Test pulses injected on calibration capacitors allow the cross-calibration of the electronics channels.

The tests of irradiated detectors were made at around -25 ^{o}C, in order to minimize the noise component coming from the leakage current. In these conditions the noise is dominated by the detector capacitance. The signal to noise ratio varies between 6:1 and 7:1 depending on the detector capacitance and the charge loss due to radiation damage.

The error on the charge measurement is about 5%, dominated by systematic uncertainties arising from the detector thickness, the timing of the electronics, the correction for the correlated noise and the fit of the most probable value of the Landau distribution.

Irradiated and non-irradiated detectors were also tested with minimum ionizing particles from the CERN SPS using the same electronics. The data confirm the laboratory results [16].

3.3 Irradiation facilities

3.3.1 The Dubna reactor

About 40 detectors were irradiated with neutrons at the pulsed reactor in Dubna [17] to fluences between 0.6 x 10^{14} n/cm^2 and 2.3 x 10^{14} n/cm^2, some in several steps. The fast neutron flux is equal to (8-10) x 10^9 n/(cm^2 s), which corresponds to 5 to 7 hours of irradiation to obtain the maximum fluence. The neutron fluence is estimated from the activation of threshold detectors and gives an uncertainty of about 10%.

The sensors are not biased during the irradiation. They are stored at a temperature below -3 ^{o}C immediately after, but they are out of the freezer during the transportation to CERN, which, including customs formalities, takes about 30 hours. They are partially annealed during this time.

3.3.2 The Proton Synchrotron at Cern

About twenty detectors were irradiated with 24 GeV/c protons at the CERN PS to fluences between 2.8 x 10^{14} p/cm^2 and 3.2 x 10^{14} p/cm^2. The sensors were biased to 150 V and cooled to –7 ^{o}C during the irradiation and stored at temperatures below -3 ^{o}C immediately after and taken out into ambient conditions only for measurements.

Fluences equivalent to 10 years of CMS operation can be achieved in approximately 6-10 days. The error on the fluence is of the order of 6% [18].

4 RESULTS

4.1 Capacitance measurements

Originally the Preshower sensors had a total area of 60 x 60 mm^2 and a pitch of 1.81 mm.This size was increased to 63 x 63 mm^2 and the pitch to 1.9 mm in order to take advantage of the whole 4" wafer surface. At the same time we have varied the gap between strips searching for an optimum from the noise, the cross-talk and the charge collection uniformity points of view. We also designed a detector with a constant pitch, but with 2 different interstrip gaps to be able to measure directly the interstrip capacitance. Table 1 summarizes the geometrical parameters of the tested detectors and the results.

Detector #	l	p	d	g	V	$C_{backplane}$	C_{total}	Fluence
	[mm]	[mm]	[mm]	[mm]	[V]	[pF]	[pF]	[10^{14} cm^{-2}]
RTD43-23	63	1.90	.305	.06	200	41.9	50.7	0
RTS24-21	63	1.90	.282	.06	200	45.5	51.8	0
RTD42.7	63	1.90	.305	.06	300	42.1	50.4	0
RTS24-7	63	1.90	296.	.06	200	43.8	50.2	0
RTS6-6	63	1.90	.310	.06	200	43.1	51	0
Takion19	60	1.81		.05	150	37.7	46.6	0
Takion19	60	1.81		.16	150	37.7	41.5	0
Hamamatsu19	60	1.81	.310	.11	200	37.1	43	0
India1	60	1.81	.310	.12	200	36.9	41.3	0
India2	60	1.81	.310	.12	200	37.1	40	0
ElmaA'-2	60	1.81	.390	.12	100	30.3	38	0
Dem2-4	60	1.81		.11	140	38.7	42.4	0
D8-25-O	63	1.90	.280	.06	400	42.0	48	2.9 p
Takion18	60	1.81	.320	.05	400	37.3	42.9	1.18 n
Takion18	60	1.81	.320	.16	400	37.3	38.2	1.18 n
ElmaA'-1	60	1.81	.370	.12	200	30.3	35.1	2.8 p
Hamamatsu5	60	1.81	.310	.11	300	37.2	43.2	1.35 n
DemA3<100>	60	1.81		.11	400	37.2	41.3	2.9 p
Dem41<111>	60	1.81		.11	400	37.2	41.6	2.9 p
DemN5	60	1.81	.370	.16	600	31.3	35.9	2 n

Tab. 1. Detectors parameters and the results of capacitance measurements. l is the strip length, p is the pitch, d is the wafer thickness, g is the gap between p+ strips and V is the bias voltage.

Looking at the backplane capacitance one can see three groups of values. The lowest one, around 30 pF, corresponds to 60 x 60 mm^2 sensors, made on wafers .37 mm to .39 mm thick. The second group, around 37 pF, are the detectors of the same area, but of an average thickness of .28 mm to .32 mm. One can see that by increasing the wafer thickness from the standard .3 mm to .38 mm one gains 7 pF in the capacitance. This gain would, however by accompanied by an increase of the bulk current, quite important on irradiated sensors. The operating voltage would also be higher, so the overall result would rather be negative (see also section 4.4).

The third group are the detectors of the final surface area of 63 x 63 mm^2, which have an average backplane capacitance of 43.2 pF, although their average thickness is also .3 mm. This increase is due to an increased surface of the strip.

Wafers cut along the <111> crystal plane have an order of magnitude more unsaturated bonds than those which are cut along the <100> plane. These bonds contribute to the density of the oxide charge, which can in turn increase the interstrip capacitance. Authors of reference [13] report that, although there was no difference in the interstrip capacitance on non irradiated sensors, the capacitance on detectors made on <111> wafers increased considerably after irradiation. In order to study this effect we have processed <111> and <100> wafers of similar resitivity, between 3 kΩcm and 5 kΩcm, in one run and evaluated the parameters. Table 1gives the strip capacitance of detectors DemA3<100> and Dem42<111>, made on <100> and <111> wafers respectively, and both irradiated to 2.9 x 10^{14} p/cm^2. They have the same backplane capacitance and their total capacitance is almost identical. From this we deduce that for the Preshower geometry there is no difference in the interstrip capacitance for these two orientations of the crystal lattice, even after irradiation.

4.2 Interstrip gap optimization

The geometry of the Preshower sensors is fairly simple and the strip pitch is fixed by the wafer size. The only parameter that could be optimized was the p^+-p^+ distance. It influences the capacitance, hence the noise and the cross talk between strips, and the uniformity of the charge collection in the region between strips.

The interstrip capacitance can be derived from measurements on two sensors, Takion 18 and 19, which have two regions: one with a 0.05 mm p^+-p^+ gap and one with a 0.16 mm gap. The difference of the total capacitance between these two regions is 5.1 pF and 4.7 pF for Takion 18 and Takion 19 respectively. They are in close agreement with calculated values of 4.9 pF [6] and 4.8 pF [7].

The higher capacitance on detectors with a smaller interstrip distance is confirmed by the measurement of the signal cross talk between channels. Figure 8 shows the relative signal measured on one strip when the particle crossed the neighboring strip as a function of the p^+-p^+ distance. While for gaps bigger than .12 mm this signal is of the order of 3.5%, it increases to almost 7% for a .05 mm gap.

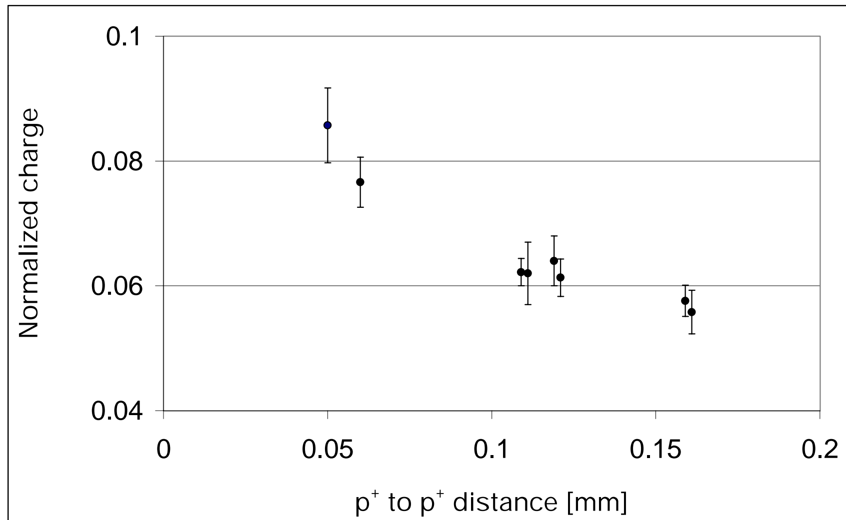

Figure 8: Relative signal measured on a strip, when the particle crossed the neighboring strip, as a function of the p^+-p^+ distance.

These arguments indicate that a large interstrip distance is more favorable. Looking however at the charge collected in the region between strips, figure 9, one sees that on detectors with a large interstrip gap the charge loss is about 15%, compared to 2% on detectors with a small interstrip distance.

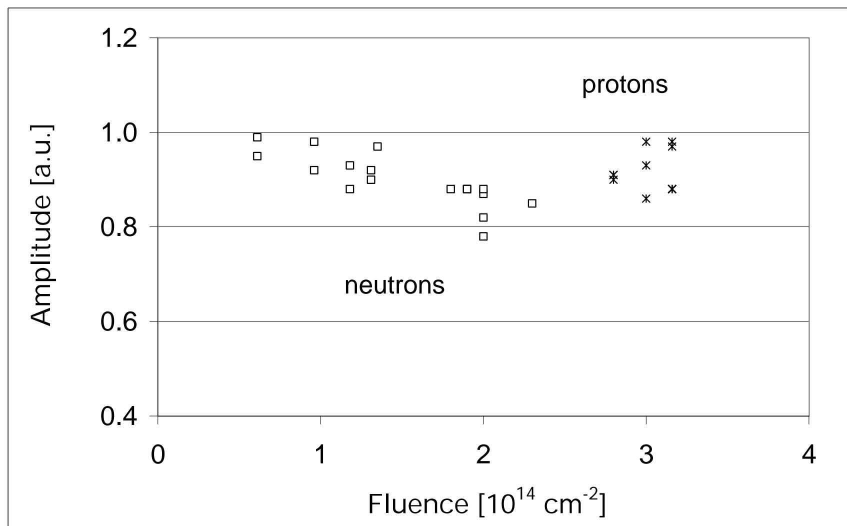

Figure 9: Normalized charge collected in the interstrip region measured with particles and using a precise beam telescope to define the position of the track.

4.3 Leakage current and full depletion voltage of irradiated detectors

Figure 10 shows as an example the total leakage current at -5°C of three Preshower sensors irradiated to 0.6 x 10^{14} n/cm^2, 1.4 x 10^{14} n/cm^2 and 2 x 10^{14} n/cm^2.

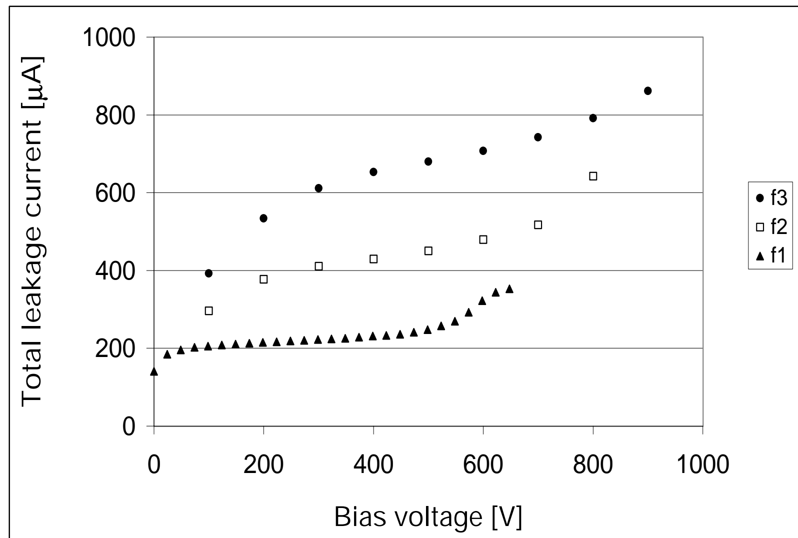

Figure 10: Total leakage current at -5 °C as a function of voltage for three sensors irradiated with neutrons: f1 = 0.6×10^{14} n/cm^2, f2 = 1.4×10^{14} n/cm^2, f3 = 2×10^{14} n/cm^2.

One can see that the leakage current increases progressively with the fluence to attain a value of about 620 µA at 300 V after 2 x 10^{14} n/cm^2, as expected (see section 2). An average value of the current related damage constant α, obtained from our measurements, is 3.2 x 10^{-17} A/cm, comparable to the values reported by other groups [2], [3], taking into account the partial annealing of the sensors.

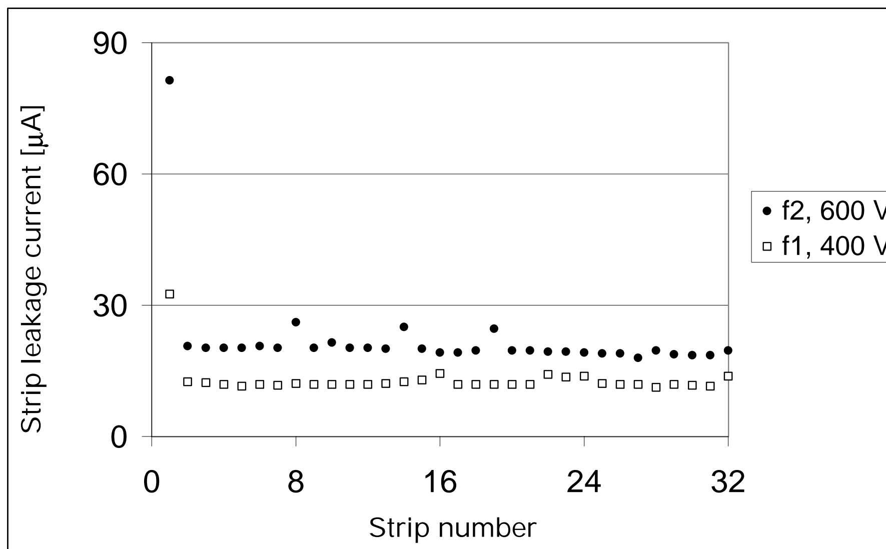

Figure 11: Strip leakage current for two irradiated sensors: f1 = 1.4×10^{14} n/cm^2, f2 = 2×10^{14} n/cm^2.

Figure 11 shows the strip leakage current for two detectors irradiated to 1.4 x 10^{14} n/cm^2 and 2 x 10^{14} n/cm^2, measured at 400 V and 600 V respectively. One sees that except the edge strips, the distribution is uniform, proving that it comes only from the bulk.

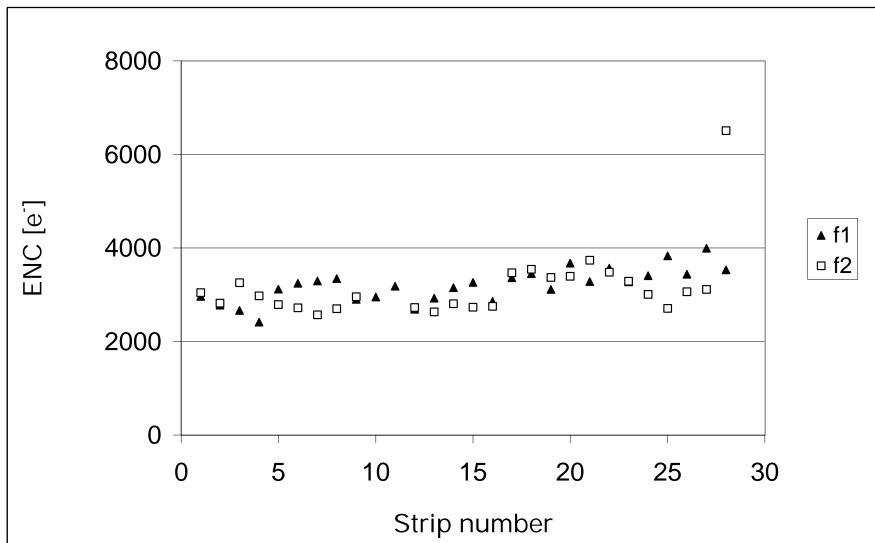

Figure 12: Noise measured with the SCT32 chip: before irradiation at 170 V, after irradiation to f2 = 3.2×10^{14} p/cm^2 at 400 V.

Figure 12 shows the noise for one sensor before and after irradiation to 3.2×10^{14} p/cm^2 measured at 170 V and 400 V, respectively. The measurement after irradiation was done at -25 ^{o}C to reduce to noise component from the leakage current.

Figure 13 shows the summary of our measurements of the full depletion voltage as a function of fluence for detectors irradiated with neutrons between 0.6 x 10^{14} 1/cm^2 and 2.3 x 10^{14} 1/cm^2 and protons between 2.8 x 10^{14} 1/cm^2 and 3.2 x 10^{14} 1/cm^2. All detectors have undergone type inversion. The depletion voltage for detectors irradiated with neutrons increases linearly with the fluence with a rate of about 190 V per 10^{14} n/cm^2. A similar value was measured by the authors of reference [4].

The full depletion voltage of detectors irradiated with protons to an average fluence of 3 x 10^{14} 1/cm^2 is equivalent to that of detectors irradiated with neutrons to a fluence of 1.53 x 10^{14} 1/cm^2. It was reported in several pub-

lications that the protons are less damaging, considering the change of the effective doping concentration [2], [4].

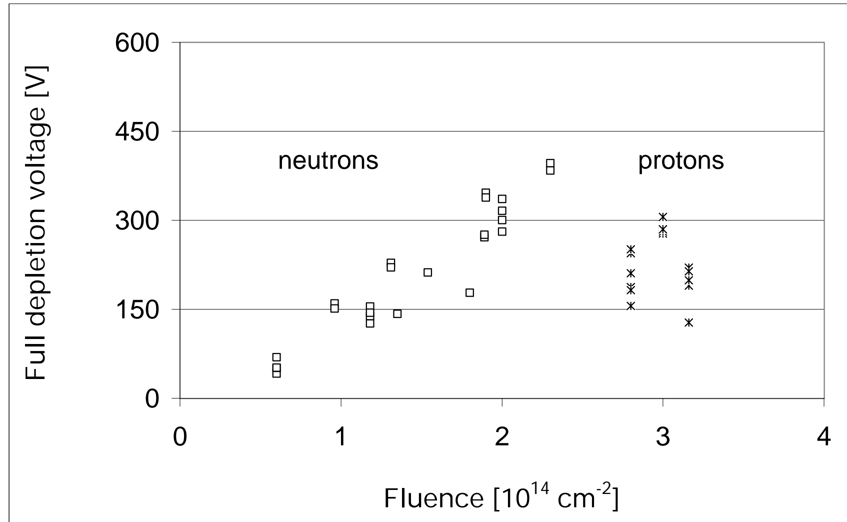

Figure 13: Full depletion voltage calculated from the backplane capacitance measurement.

4.4 Charge loss after irradiation

The Preshower detector, unlike the tracking detectors, requires a measurement of the absolute charge deposited in silicon and it is both the signal and the noise, and not only the signal-to-noise ratio, that determine the performance. We have therefore to monitor carefully the charge loss during the experiment. This effect was studied for all irradiated detectors

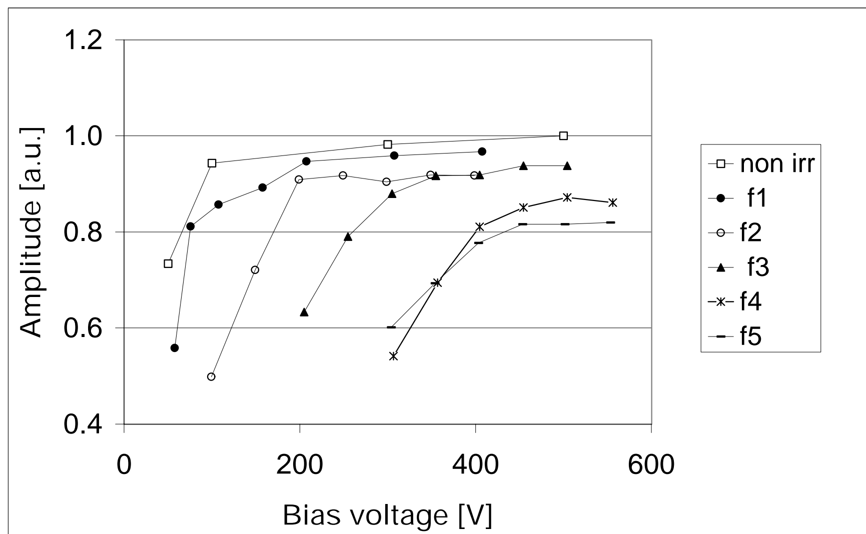

Figure 14: Normalized charge collected from irradiated detectors as a function of bias voltage: f1 = 0.6×10^{14} n/cm^2, f2 = 0.96×10^{14} n/cm^2, f3 = 1.31×10^{14} n/cm^2, f4 = 1.9×10^{14} n/cm^2, f5 = $2. \times 10^{14}$ n/cm^2.

Figure 14 shows typical curves obtained with .3 mm detectors made on high resistivity silicon. One sees that the plateau starts at higher and higher voltages and the amplitude at the plateau decreases with the fluence.

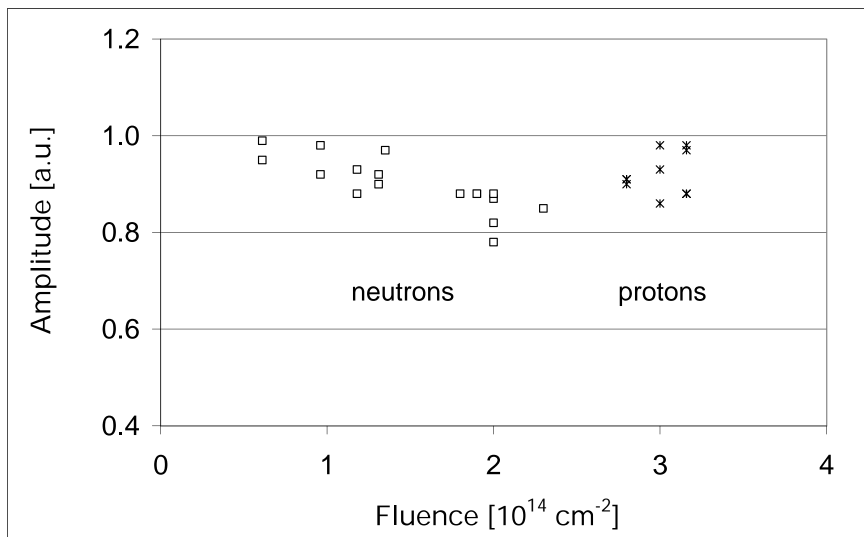

Figure 15: Normalized amplitude measured on irradiated sensors as a function of fluence.

The signal loss is due to charge trapping in damaged silicon. Figure 15 shows the normalized amplitude for proton and neutron irradiated detectors as a function of particle fluence. For neutron irradiated detectors we observe an 8.5% charge loss per 10^{14} n/cm^2. Similar values were measured on diodes [10], [11] and calculated [12].

The charge loss for detectors irradiated with protons, about 8.4%, for an average fluence of 3 x 10^{14} p/cm^2 is equivalent to damage caused by about 1 x 10^{14} n/cm^2.

Among the Preshower sensors produced in the past three years, we had about 10 made on thicker wafers, .37 mm to .39 mm. Using thicker wafers is tempting from two points of view: the charge deposited, proportional to the thickness, is higher and the noise, proportional to the capacitance and inversely proportional to the thickness, is lower. We irradiated these detectors and found, that they require a very high voltage to reach the charge collection efficiency plateau. Figure 16 shows the measured amplitude, normalized to .3 mm, as a function of voltage for four sensors, two thick and two thin and irradiated to fluences of 0.6 x 10^{14} n/cm^2 and 2 x 10^{14} n/cm^2. One can see that the thicker detectors require 80 V to 100 V more to reach the plateau.

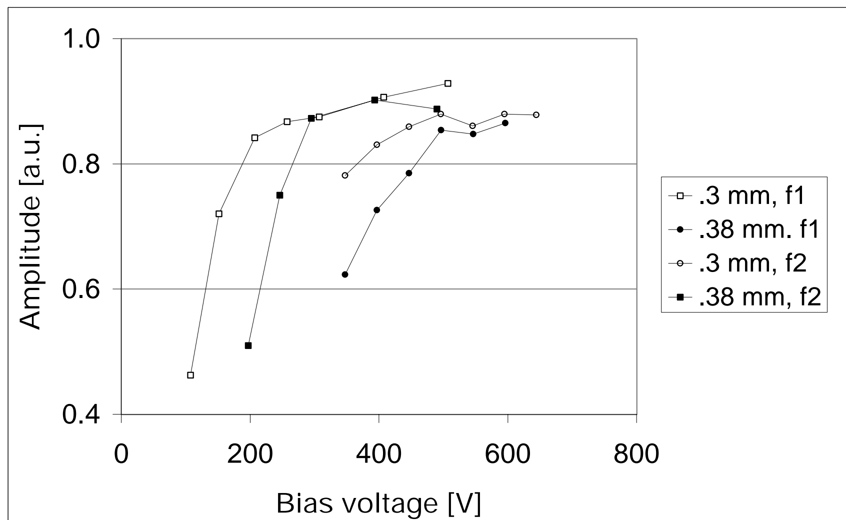

Figure 16: Comparison of charge collected from thin and thick detectors irradiated to two fluences: f1 = 0.6×10^{14} n/cm^2, f2 = 2×10^{14} n/cm^2.

Thicker detectors would dissipate about 60% more power, as their volume leakage current is also higher, making

the cooling more difficult. The higher leakage current contribution to the noise would compensate the gain from a lower capacitance. Moreover, the PACE electronics has a limited dynamic range and would not take full advantage of the increased signal. These considerations lead us to the conclusion that a thickness above .37 mm is too high for our purposes.

The effective doping concentration is a function of fluence and of the initial donor and acceptor atom concentrations [4]. For a higher donor atom concentration, a longer irradiation time is required before the acceptor level reaches the donor level and the detector becomes intrinsic. One expects therefore lower full depletion voltage after inversion on low resistivity sensors. We ordered from one manufacturer 5 sensors on 1.3 kΩcm silicon and requested that they be produced using the same masks and in the same process as the 15 sensors made on 4 kΩcm silicon. Figure 17 shows the normalized amplitude measured on four irradiated detectors: A and C are made on 4 kΩcm initial resistivity silicon, and B and D on 1.3 kΩcm resistivity. Detectors A and B were irradiated with protons to 3 x 10^{14} cm^{-2} and C and D with neutrons to 2 x 10^{14} cm^{-2}. One can see that the detectors irradiated with protons reach the plateau at practically the same voltage. For the neutron irradiated low resistivity detector the gain in the operating voltage is clear as it reaches the plateau at about 100 V lower voltage than the other detector. But, as we shall see in section 5.3 , obtaining good initial parameters on low resistivity wafers is difficult (see figure 23) and we decided to use wafers of a resistivity between 3 kΩcm and 4 kΩcm.

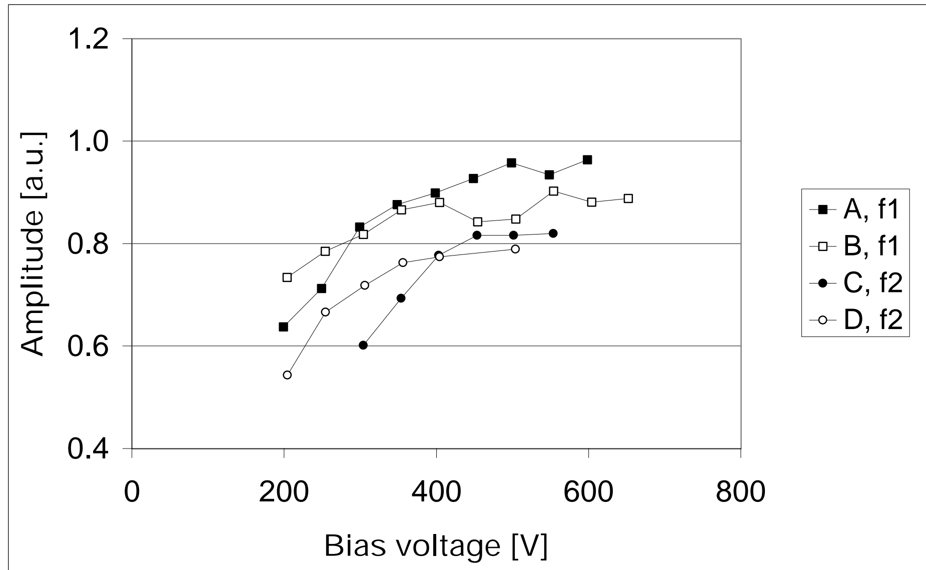

Figure 17: Normalized amplitude measured on low and high resistivity, irradiated sensors: detectors A and C are made on 4 kΩcm initial resistivity silicon, and sensors B and D on 1.3 kΩcm resistivity. Fluence f1 = 3×10^{14} p/cm^2 and f2 = 2×10^{14} n/cm^2.

4.5 Operating voltage

Operating non irradiated or irradiated, but not inverted sensors, at the full depletion voltage, calculated from the C-V curve, guarantees a good charge collection efficiency. The results presented in section 4.4 show, however, that for inverted sensors one needs a higher operating voltage, V_{oper}. Figure 18 shows the voltage necessary to reach full charge collection as a function of fluence for sensors of high resistivity and .3 mm thick, irradiated with neutrons in the range from 0.6x10^{14} 1/cm^2 to 2.3×10^{14} 1/cm^2 and with protons between 2.8×10^{14} 1/cm^2 and 3.2 $\times 10^{14}$ 1/cm^2. All detectors are inverted.

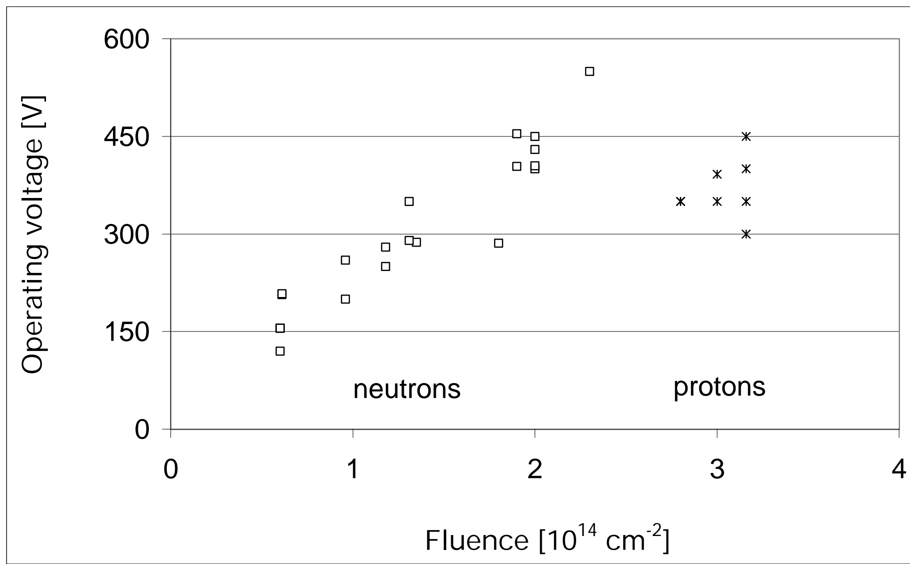

Figure 18: Voltage necessary to reach the full charge collection as a function of fluence for detectors irradiated with neutrons in the range from 0.6×10^{14} cm^{-2} to 2.3×10^{14} cm^{-2} and with protons between 2.8×10^{14} cm^{-2} and 3.2×10^{14} cm^{-2}. Only sensors made on high resistivity, .3 mm thick wafers are plotted.

One observes a linear increase of the operating voltage, with a rate of about 200 V per 10^{14} n/cm^2, similar to the slope of the full depletion voltage as a function of fluence (see figure 13). For the proton irradiated sensors, the damage is lower and the operating voltage for a fluence of 3×10^{14} p/cm^2 is equivalent to a fluence of about 1.5×10^{14} n/cm^2.

Figure 19 shows the difference V_{oper} -V_{fd} as a function of fluence for proton and neutron irradiated and inverted sensors. One sees that between 50 V and 150 V of over depletion are necessary to have a good charge collection efficiency. For safe operation, one should require the breakdown voltage to be at least 200 V higher than the full depletion voltage.

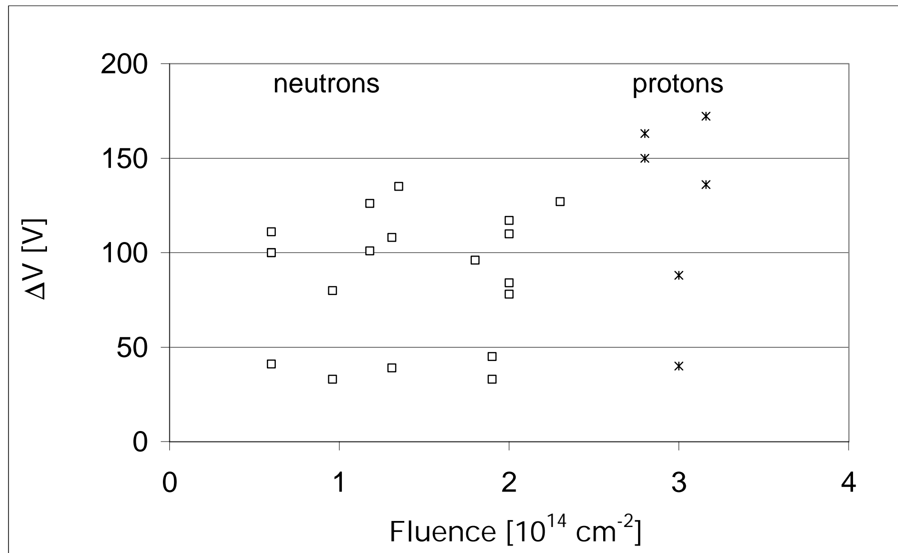

Figure 19: Difference of the operating voltage and the full depletion voltage, determined from the C-V curve, as a function of fluence for proton and neutron irradiated and inverted sensors.

4.6 Long term measurement

In order to make sure that the sensors can operate in stable conditions after the irradiation, we prepared a set-up in

which the sensors could be biased and cooled to around -2 ^{o}C and monitored regularly. Figure 20 shows the leakage current as a function of voltage of two sensors, irradiated to 1.35×10^{14} n/cm^2 and to 1.8×10^{14} n/cm^2. The voltage applied was 150 V for the first 70 days, and then it was increased 300 V. One sees that the current was not stable during the first couple of days, but then it stabilized and remained constant over a period of 4 months.

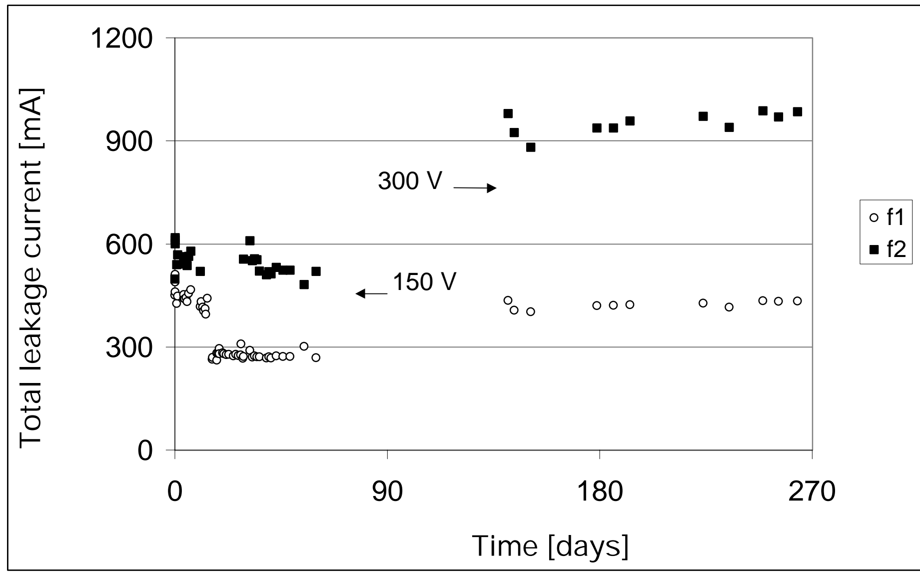

Figure 20: Leakage current as a function of time for two detectors irradiated to 1.35×10^{14} n/cm^2 (full squares) and to 1.8×10^{14} n/cm^2 (open squares), measured at -2°C.

5 Technological issues

5.1 Double sided and single sided polished wafers

During the research and development phase of our project we focussed our efforts on technological issues which could have an impact on the cost of the project, either by reducing the production cost or by increasing the yield. Most manufacturers use silicon wafers polished on both sides, as it was clear from the beginning that a good quality of the backplane is important in reducing the back-plane injection current. But double sided polished wafers are more expensive.We have made a comparison of 24 single sided polished and 40 double sided polished wafers in one production run. Figure 21 shows the leakage current as a function of voltage for 15 and 32 accepted sensors, respectively. One sees that sensors made on single sided polished wafers are at least as good as those made on double sided polished wafers.

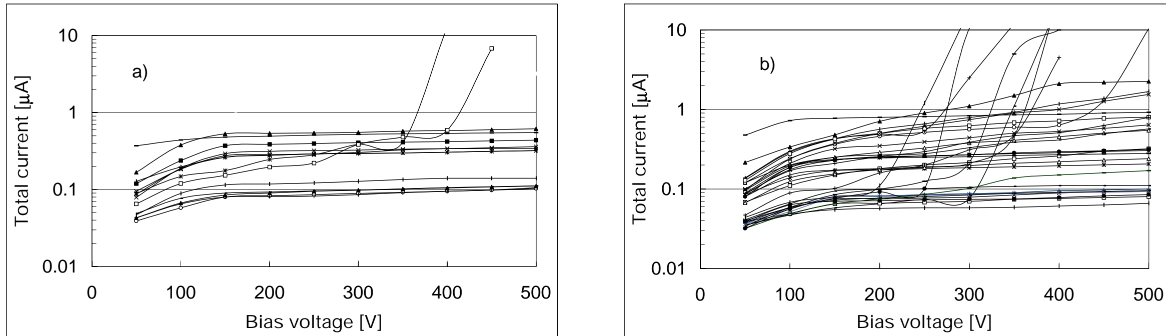

Figure 21: I-V characteristics of sensors made on single sided (a) and on double sided (b) polished wafers, all produced in the same run.

5.2 Backplane doping

A change of the technology of the backplane phosphorus implantation increased the yield dramatically. A thicker n^+ layer obtained by a double implantation increases considerably the breakdown voltage. Figure 22 shows the I-V characteristics for sensors from two production runs: one of 45 sensors with 1μm thick n^+ layer (a) and the second one of 47 wafers with a 3 μm thick layer (b). Characteristics of 31 and 36 sensors, respectively, are plotted. The quality improvement is remarkable.

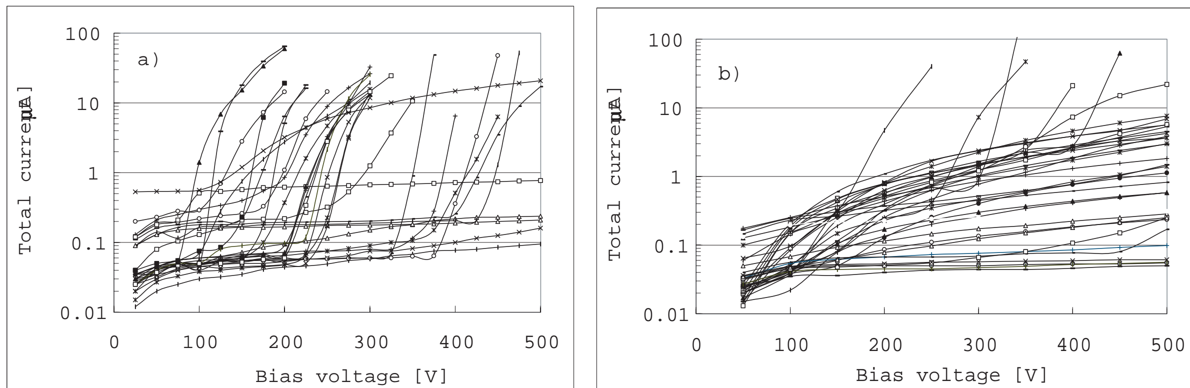

Figure 22: I-V characteristics of sensors with 1 μm and 3 μm phosphorus implantation (a and b respectively).

A large fraction, 78%, of the sensors with a 1μm thick n^+ layer have a breakdown voltage lower than 500 V. On the other hand, more than 80% of sensors with the thicker layer have a breakdown voltage in excess of 500 V.

A thick backplane implantation protects the bulk from the backplane injection and diffusion currents at high voltages. Defects at the silicon surface generate charge carriers, which diffuse to the space charge region, if their life-

time is long and if the n^+ implant layer is relatively thin. This current adds to the bulk current and may become important at high voltages. If, however, the n^+ layer is thick, the carriers will have a good chance to recombine before reaching the bulk.

The same explanation is valid for the observed phenomenon of sensor breakdown improvement after irradiation [19]. We noticed that the sensors with a thin phosphorus layer and a relatively low breakdown voltage can hold up to 600 V after being strongly irradiated. In this case it is the reduction of the carrier lifetime, that inhibits them from diffusing into the space charge region.

5.3 Low resistivity silicon

Figure 23 shows the leakage current as a function of voltage and the inverse square of the capacitance as a function of voltage (a and b respectively) of the low resistivity sensors.

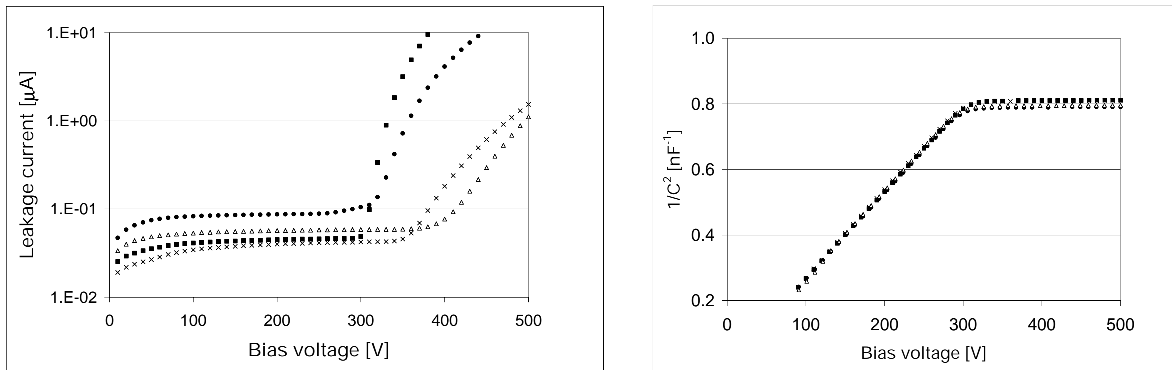

Figure 23: Sensors made on a 1.3 kΩcm silicon: a) Leakage current as a function of voltage, b) inverse square capacitance as a function of voltage

One sees that the full depletion voltage is about 300 V and that none of the sensors can hold a voltage higher than 100 V above the full depletion, while all high resistivity sensors produced in the same run had a breakdown voltage higher than 500 V. It seems that it is more difficult to produce a good detector on a low resistivity material. As we have shown in section 4.4 the gain after an irradiation to a full expected fluence is less than 100 V. Given the fact that we have reached good performance with medium and high resistivity sensors, we aim for a resistivity in the range between 3 kΩcm to 4 kΩcm.

6 SPECIFICATIONS

The research and development program conducted during the past three years has allowed us to define the specifications for the production. The preliminary values and conditions are listed in table 2.

parameter	**value**
wafer size	4 “
thickness	.32 ± .01 mm
resistivity	3 kΩcm - 4 kΩcm
polishing	single sided
n^+ layer thickness	> 2.5 µm
total area	63 x 63 mm^2
number of strips	32
number of guard rings	4
strip pitch	1.9 mm
p^+ strip width	1.78 mm
Al strip width	1.8 mm
I_{total} at V_{fd}	< 5 µA
I_{total} at V_{fd} + 150 V	< 10 µA
V_{br}	> 300 V

Tab. 2. Preliminary specifications of the Preshower sensors.

To this list we should add the requirement that we accept no more than one strip with a current in the range 1 µA < I < 5 µA.

The required breakdown voltage of 300 V might seem low in view of the presented results. But a large majority of our sensors will be at a radius where the fluence will never reach 1.5 x 10^{14} n/cm^2 and for which the operating voltage will be below 300 V. Given the excellent parameters of the 250 sensors already produced by one manufacturer, we are confident that we will be able to select enough sensors with a breakdown voltage exceeding 500 V and which we will place in the central ring, close to the beam pipe.

We should also mention that we observed an increase of the breakdown voltage after irradiation on all sensors of low initial quality [19]. It is due to a reduction of carrier lifetime, which limits the diffusion of carriers generated at the backplane surface and injected into the depletion region.

7 SUMMARY and CONCLUSIONS

We presented the results of three years of research and development on silicon sensors for the CMS Preshower. The main goal was to arrive at a design and technology which would guarantee a good detector performance during ten years of LHC operation.

The key points in the design are the structure of the guard rings and the metal lines extending outside the p^+ implants. Both reduce the maximum field around the strips and, at the same time, increase the breakdown voltage.

Concerning the technology, we found that polishing the wafers on the ohmic side is not necessary, as we did not see any improvement of the leakage current or the breakdown voltage. On the other hand we found that a deep and uniform Phosphorus implantation increases considerably the breakdown voltage and the yield.

During the design phase we also optimized the interstrip gap, an important parameter, governing the uniformity of the charge collection and the capacitance, hence the cross talk and the noise.

Over 60 sensors were irradiated with protons or neutrons and thoroughly tested before and after irradiation. Sensors designed and produced following the above mentioned procedure have a very low initial current and a breakdown voltage of over 500 V before and after irradiation.

As a result of this work we have clear specifications concerning the design and the technology and we are ready to start the production. The 5000 sensors will be produced in four centers over a period of three years. We plan to irradiate systematically 1% of the produced sensors to monitor their quality. A test set-up, composed of a 32-pin probe card and a switching matrix, allowing an automatic measurement of the current and the capacitance, is ready for acceptance test.

Acknowledgments

The authors would like to thank the Preshower group for their help in writing the paper and, in particular, Edwige Tournefier for providing figure 1, Evgenij Zubarev for drawing the layout and the cross section of the silicon sensors, Anarbai Urkinbaev for figures 8 and 9 and Alexandre Cheremuhin for his help in certain measurements. The greatest thanks should go to Dave Barney, who patiently proof reads all our notes.

We would also like to thank V. Golikov and E. Kulagin for irradiating silicon sensors and for monitoring the neutron fluence.

Discussions with A. Sidorov, N. Egorov and S. Golubkov on technological issues were very useful.

8 References

[1] CMS ECAL Technical Design Report, CERN/LHCC 97-33

[2] A. Chilingarov et al., Nucl. Instr. Methods, vol. A 360 (1995) 432

[3] B.C. MacEvoy, “Defect kinetics in silicon detector material for applications at Large Hadron Collider”, Thesis, RAL-TH-97-003

[4] G. Lindstrom et al., ROSE/TN/2000-03

[5] D. Passeri et al., CMS CR 1999/030

[6] R. Shivpuri, Dehli University, private communication

[7] J. Moussa, A. Kyriakis and D. Loukas, “Potential Profile, Capacitance and Charge Collection in the Silicon Detector of the CMS Preshower”, private communication

[8] P. Aspell, “The design of the Pace integrated circuit for the LHC CMS Preshower Detector system”, Open University degree thesis, No. T401, Walton Hall, UK, 1997

[9] .P. Aspell et al., “Delta: A charge sensitive front-end amplifier with switched gain for low noise, large dynamic range silicon detector readout”, presented at the 8th Pisa Meeting on Advanced Detectors, May 2000, Isola d’Elba, submitted to Nucl. Instr. Methods

[10]L. Beattie et al., “Charge collection efficiency in heavily irradiated silicon diodes”, Nucl. Instr. Methods vol. A 412 238–246 (1998).

[11]C. Leroy et al., Proc. IVth Int. Conf. on Calorimetry in High Energy Physics, La Biodola, Isola d’Elba, Italy, 1993, eds. A. Menzione and A. Scribano, Singapore: World Scientific, 1994, p. 627.

[12]C. Leroy et al., “Study of charge transport in non-irradiated and irradiated silicon detectors”, Report CERN-EP 98–105.

[13]S. Braibant et al., CMS Note 2000/011

[14]F. Anghinolfi et al., “SCTA – A rad-hard BiCMOS analog readout ASIC for ATLAS semiconductor tracker”, IEEE Trans. Nucl. Sci., vol. 44, No. 3, 298–302 (1997).

[15]Ph. Bloch et al., “High voltage performance of silicon detectors irradiated under bias”, Nucl. Instr. Methods, vol. A 439 344–348 (2000).

[16]P. Bloch et al., Performance Study of Non-Irradiated Prototype Silicon Preshower Samplers for CMS, CMS NOTE-2000/042

[17]A. Cheplakov et al., “Radiation hardness of GaAs preamplifiers for liquid argon calorimetry at LHC”, MPI Report, PhE/96–15.

[18]E. León-Florián et al., “Particle fluence measurements by activation technique for radiation damage studies”, Report CERN-ECP-95–15.

[19]Ph. Bloch et al., “Improvement of silicon detectors breakdown voltage after irradiation”, submitted to IEEE Transactions on Nuclear Science